

Evaluation of SVM classification of metallic objects based on a magnetic-dipole representation

Juan Pablo Fernández,^a Benjamin Barrowes,^b Kevin O’Neill,^{a,b} Keith Paulsen,^a
Irma Shamatava,^a Fridon Shubitidze,^a and Keli Sun^a

^aThayer School of Engineering, Dartmouth College, Hanover, NH 03755-8000, U.S.A.;

^bU.S. Army Corps of Engineers, Engineer Research and Development Center,
Hanover, NH 03755, U.S.A.

ABSTRACT

In the electromagnetic-induction (EMI) detection and discrimination of unexploded ordnance (UXO) it is important for inversion purposes to have an efficient forward model of the detector-target interaction. Here we revisit an attractively simple model for EMI response of a metallic object, namely a hypothetical anisotropic, infinitesimal magnetic dipole characterized by its magnetic polarizability tensor, and investigate the extent to which one can train a Support Vector Machine (SVM) to produce reliable gross characterization of objects based on the inferred tensor elements as discriminators. We obtain the frequency-dependent polarizability tensor elements for various object characteristics by using analytical solutions to the EMI equations. Then, using synthetic data and focusing on gross shape and especially size, we evaluate the classification success of different SVM formulations for different kinds of objects.

Keywords: Unexploded ordnance (UXO), magnetoquasistatics, machine learning, Support Vector Machines

1. INTRODUCTION

The presence of unexploded ordnance (UXO) in a variety of settings, from decommissioned firing ranges to former World War battlefields to countries afflicted with civil war or fighting insurgencies, constitutes a pressing environmental and humanitarian problem.¹ It is estimated that some 10% of artillery containing energetics fail to explode upon impact. This high “dud rate,” combined with the sheer numbers of ordnance used around the world, has alarming consequences: millions of acres of land that cannot be inhabited or worked, hundreds of people killed or maimed every year by objects that explode decades after being fired, contaminated watersheds and environmental havens, and substantial amounts of money spent in land rehabilitation.

The main reason for the high cost of UXO identification—most of it carried out using ground-penetrating radar¹ or wideband electromagnetic-induction (EMI) detectors²—is the high false-alarm rate: *i.e.*, the need to have to treat every buried piece of metal as potentially dangerous, be it actual UXO, scrap, rocks with high metal content, old nails, or any such innocuous items. In other words, the difficulty is not one of detection but one of discrimination. One could think that this is really not that difficult, since unexploded ordnance, being bodies of revolution with smooth contours, would be expected to exhibit symmetries not present in irregularly shaped objects. However, this simplistic picture is complicated by many factors. Predictable ones are the small signal-to-clutter ratio and the fact that the classification and discrimination of UXO, like other inverse problems, is in general ill conditioned and plagued by non-uniquenesses. Besides, the EMI response of UXO is affected by their location and orientation relative to the detector. Also, UXO in general have realistic, finite electromagnetic parameters and thus are in a régime where few approximations or idealizations can be made. Not least important, many UXO are actually composite objects, consisting of two or more interlocking pieces of different materials that yield differing signals under differing excitation and thereby present the detector and discrimination algorithms with competing and possibly conflicting pieces of information.

On the one hand, then, quite sophisticated forward models are needed to yield a reasonable characterization of buried UXO; on the other, one would hope to obtain good results within a reasonable timespan, preferably in real

Further author information: (Send correspondence to J.P.F.)

J.P.F.: E-mail: jpfb@dartmouth.edu, Telephone: 1 603 646 1487

time. To find a compromise between these clashing aims, in this work we present some considerations relating to a preliminary version of the first stage of a possible multi-stage discrimination algorithm. This algorithm would attempt to distinguish promising UXO candidates from other buried items by studying their response to the primary field of an EMI detector in the light of increasingly elaborate models, both analytic³⁻⁵ and numerical,^{6,7} while striving to identify the electromagnetic signatures of potentially dangerous hidden objects. In intermediate steps, a classification procedure could assist and complement these forward models by dismissing false alarms early in the process using the results of simple but fast discriminators.

As an initial guess we consider that an object responds to the impinging field as would an anisotropic, infinitesimal magnetic dipole characterized by a magnetic polarizability tensor.^{1,8} The dipole model has had limited success at providing robust discriminators for UXO when used on its own. However, any metallic object subjected to a primary field develops a dipole moment that must in some way be a result of its characteristics, even if the infinitesimal dipole model is inadequate for unique predictions of behavior under other excitations. Despite its limitations, which stem from its simplicity, the dipole model can represent a first stage in discrimination by potentially enabling us to sort UXO candidates according to their sizes, shapes, or electromagnetic properties.

To classify the polarizability data we use Support Vector Machines (SVMs), an automated “learning by examples” method that by now is well understood theoretically⁹ and readily available in fully fledged, thoroughly tested, and wholly functional implementations.^{10,11} SVMs have proved to be a trustworthy and efficient classification algorithm in fields where the establishment and identification of patterns is important: handwriting and facial recognition, bioinformatics, and text categorization, among others. In the context of UXO discrimination, SVMs are being used ever more often, for example to train computers to draw “risk maps” of areas that might be contaminated with ordnance.¹² A study similar to ours¹³ has found that SVMs perform well in the classification of UXO starting from EMI and magnetometer data.

In this paper we evaluate the success of two open-source SVMs in the classification of spheres and prolate spheroids starting with exact analytical solutions to the EMI equations. In the next section we discuss the characterization of UXO by means of dipoles, concentrating on the spherical and spheroidal results that we will use in the rest of the paper. Section 3 contains a brief discussion of the features and operation of Support Vector Machines. Section 4 describes the discrimination experiments we carried out. We conclude and review some directions for future work in Section 5.

2. DIPOLE MOMENTS FOR UXO CHARACTERIZATION

EMI detectors work in the magnetoquasistatic régime, where the relatively low frequencies make it permissible to neglect displacement currents. We consider a body of finite conductivity σ and finite permeability $\mu \equiv \mu_0\mu_r$ placed in an essentially transparent, nonconducting medium and subjected to a uniform incident field \mathbf{H}_0 with time dependence $e^{-i\omega t}$. Inside the body, the total field obeys a Helmholtz-diffusion equation with complex wavenumber: $\nabla^2\mathbf{H}^{(i)} + k^2\mathbf{H}^{(i)} = 0$, where $k^2 = i\omega\mu\sigma$. Outside the body, the total field is irrotational and divergenceless, so we can express it in terms of a scalar potential Φ that obeys the Laplace equation.

After matching the boundary conditions at the surface of the object, we can find the induced dipole moment of the object by taking the far-field response and making the scalar potential outside equal to

$$\Phi = -\frac{1}{4\pi} \mathbf{m} \cdot \nabla \frac{1}{R}, \quad (1)$$

in which case we get a secondary vertical field of the form^{1,14}

$$H_z(\mathbf{r}) = \frac{1}{4\pi R^3} \left(3 \left(\frac{\mathbf{R}}{R} \cdot \hat{\mathbf{z}} \right) \left(\frac{\mathbf{R}}{R} \cdot \mathbf{m} \right) - \mathbf{m} \cdot \hat{\mathbf{z}} \right) \quad (2)$$

where $\mathbf{R} \equiv \mathbf{r} - \mathbf{r}'$, \mathbf{r} is the observation point, \mathbf{r}' is the dipole location, and the induced dipole moment \mathbf{m} defines the magnetic polarizability tensor \mathbf{B} through $\mathbf{m} = \mathbf{B}\mathbf{H}_0$. This tensor is always symmetric and, in the cases studied below, diagonal. When the tensor is nondiagonal it is always possible to find a set of principal body axes that define a polarizability ellipsoid related to the orientation of the object. The associated eigenvalues are

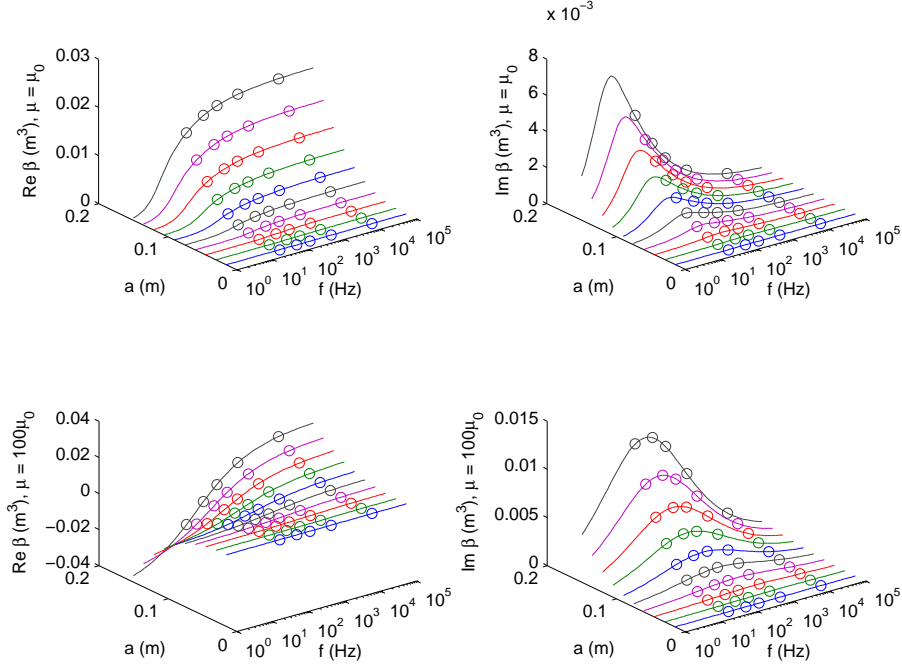


Figure 1. Induced dipole moments of spheres of increasing size due to a unit uniform field. The open circles show the GEM-3 frequencies that we use to train the SVM. The top panel corresponds to $\mu_r = 1$ and the bottom one to $\mu_r = 100$. The conductivity is 10^7 in all cases. As discussed in Sec. 4, some patterns are discernible by eye.

always real and, for bodies of revolution, degenerate. It is these elements that we will be using as discriminators in this work.

The simplest object we can consider is a sphere, which is described by a single dipole moment and whose polarizability tensor turns out to be^{3, 14, 15}

$$\mathbf{B} = 2\pi a^3 \mathbb{1} \frac{(2\mu_r + 1)(1 - ka \cot ka) - (ka)^2}{(\mu_r - 1)(1 - ka \cot ka) + (ka)^2} \equiv \beta \mathbb{1}, \quad (3)$$

where a is the sphere radius and $k^2 = i\omega\mu\sigma$ as defined above. Figure 1 shows the tensor elements for spheres with representative sizes and electromagnetic parameters.

The EMI equations have also been solved analytically for spheroids, whose shapes closely approximate those of most UXO. This exact treatment³⁻⁵ parallels that of the sphere but is considerably more involved; results corresponding to infinite conductivity,^{4, 16} applicable for high frequencies or high permeabilities, are also available. We quote some relevant results and refer the interested reader to the literature.

For definiteness we treat a prolate spheroid with semimajor axis b , semiminor axis a , and interfocal distance $d = 2\sqrt{b^2 - a^2}$; the ratio $e = b/a > 1$ is called the elongation. Maxwell's equations can be solved by separation of variables in the usual spheroidal coordinates $\eta \in [0, \pi]$, $\xi \in [0, \infty)$, and $\phi \in [0, 2\pi)$: The field inside the spheroid can be expanded in vector spheroidal wavefunctions of the first kind,¹⁷ the principal field can be expressed as a series of solutions to the Laplace equation that are regular at the origin, and the secondary field is expanded in terms of solutions to the Laplace equation that are regular at infinity:

$$\Phi_s(\mathbf{r}) = \frac{1}{2} H_0 d \sum_{m=0}^{\infty} \sum_{n=0}^{\infty} \sum_{p=0}^1 B_{pmn} P_n^m(\eta) Q_n^m(\xi) (\delta_{p0} \cos m\phi + \delta_{p1} \sin m\phi), \quad (4)$$

where $P_n^m(\eta)$ and $Q_n^m(\xi)$ are associated Legendre functions of the first and second kinds respectively and δ_{kl} is the Kronecker delta. For a given principal field, we can find the expansion coefficients B_{pmn} by matching the

normal and transverse fields at the surface of the spheroid (specified by $\xi_0 \equiv e/\sqrt{e^2 - 1}$) and can then express the polarizability tensor in terms of those. We get

$$m_z = H_0 \left(\frac{\pi d^3}{6} \right) B_{001} \equiv \beta_z H_0 \quad \text{and} \quad m_t = H_0 \left(\frac{\pi d^3}{3} \right) B_{011} \equiv \beta_t H_0 \quad (5)$$

for the induced axial and transverse dipole moments.

At high frequencies it can be assumed that the spheroid is almost a perfect conductor, and, as a consequence, the fields in its interior are nonzero only in a thin layer beneath the surface and are essentially normal to it. In this Small Penetration-Depth Approximation (SPA), the general spheroidal equations become simpler; the dipole moments they predict are in general very similar to their exact counterparts. This adds a slight inconsistency to our data, even though the two estimates differ only by a few percent, a minute distortion compared to that caused by measurement errors in the field.

3. SUPPORT VECTOR MACHINES

Within the context of learning machines (*i.e.*, programs that can be trained by feeding them a series of observations and their corresponding yes-or-no “answers” and can then use this training to make generalizations and predictions) Support Vector Machines (SVMs)^{9, 18, 19} have become increasingly popular for a variety of reasons. Not only do they require no *a priori* knowledge about the procedure that generated the data, they are based on the solid theoretical framework of statistical learning theory, which permits the design of optimal classifiers, they are sparse, which allows them to solve large problems quickly and with reasonable memory requirements, and they do their search by means of a constrained quadratic optimization routine that is simple and reliable and encounters no local optima.

Starting with a set of training observations $\{\mathbf{x}_i, y_i\}$, with $\mathbf{x}_i \in \mathbb{R}^n$ and $y_i \in \{-1, 1\}$, SVMs strive to find hyperplanes of the form $\mathbf{x} \cdot \mathbf{w} + b = 0$, where \mathbf{w} is a vector normal to the hyperplane and b a scaling factor, that separate the positive examples from the negative ones by obeying

$$y_i(\mathbf{x}_i \cdot \mathbf{w} + b) - 1 \geq 0 \quad \forall i, \quad (6)$$

and, in particular, will search for the plane with the maximum margin. The *margin* M of a hyperplane is $M = d_- + d_+ = 2/\|\mathbf{w}\|$, where d_- (d_+) is the shortest distance to the closest negative (positive) example.

To find the separating hyperplane, then, it suffices to maximize M (or, equivalently, minimize $\|\mathbf{w}\|$) subject to the constraints (6), which are incorporated via Lagrange multipliers. Once we have found the hyperplane, we can make predictions: any new \mathbf{x} will belong to the class $\text{sgn}(\mathbf{w} \cdot \mathbf{x} + b)$. (On the other hand, it is possible to go beyond this binary classification and interpolate SVM decisions to obtain a probability distribution.^{12, 20})

Another parameter that enters the optimization scheme and has to be kept under control is the capacity of the learning machine—its ability to learn any training set without error.¹⁹ Too small a capacity will cause the SVM to make uninformed decisions; too large a capacity will tend to make it overfit and hence hinder its ability to generalize. More precisely: to prevent overfitting when starting from a small set of training samples, it is necessary to limit the complexity of the classifying function. (This is particularly important in the presence of noise.) It is better to have a relatively simple function that will make some mistakes than one that fits the data too tightly and will make gross misrepresentations when confronted with other samples.²¹

To that end, one can “soften the margin” by introducing slack variables ξ_i corresponding to the constraints in Eq. (6) and thus turning the problem into

$$\begin{aligned} \max_{\mathbf{w}, b, \xi} \quad & \frac{1}{2} \|\mathbf{w}\|^2 + C \sum_i \xi_i \\ \text{subject to} \quad & y_i(\mathbf{x}_i \cdot \mathbf{w} + b) \geq 1 - \xi_i, \\ & \xi_i \geq 0, \end{aligned} \quad (7)$$

where C is the capacity. This quadratic optimization problem is usually solved in its dual form.¹⁹

Support Vectors are those training points with nonzero Lagrange multipliers whose removal would change the location of the separating hyperplane. In other words, support vectors correspond to the critical points upon which the machine’s decisions hinge. When doing the classification, the SVM will only keep the information relating to the support vectors, making the problem sparse.

The decision boundaries will not be, in general, planes, since the relationships may be nonlinear; here is where kernels come in. A kernel is a mapping $\Phi : \mathbb{R}^n \mapsto \mathbb{R}^m$ that can help find the hyperplanes for nonlinear cases by embedding them in a space of higher dimensionality; the sparsity of the problem lets this dimension be very large. To introduce a kernel one replaces the scalar products in (6) by more-general scalar functions of the form

$$\mathbf{x} \cdot \mathbf{y} \rightarrow K(\mathbf{x}, \mathbf{y}) \equiv \Phi(\mathbf{x}) \cdot \Phi(\mathbf{y}); \tag{8}$$

like other authors,¹³ we have found the Radial Basis Function (RBF) kernel, given by

$$K(\mathbf{x}, \mathbf{y}) = \exp(-\|\mathbf{x} - \mathbf{y}\|^2/2\sigma^2), \tag{9}$$

to work best. The Gaussian width σ , like the capacity C , is an adjustable parameter.

Of the various available SVM implementations, we have concentrated on two: SVM^{light} by T. Joachims¹⁰ and mySVM by S. Rüping.¹¹ In what follows we will evaluate the performance of these two programs in classifying spheres and spheroids by size and shape based on their dipole moments.

4. EXPERIMENTS AND RESULTS

In the numerical experiments that follow we have kept the frequencies fixed at values typically measured by the GEM-3 detector:² $f \in \{30, 90, 210, 810, 10950\}$ Hz, shown as open circles in Fig. 1. We have avoided the highest GEM-3 frequencies, which have been found to yield unreliable results in field measurements.

As we saw in Section 2, a sphere has a single-element polarizability tensor, which depends on its size, conductivity, and permeability. As the top panels of Fig. 1 show for the case $\mu = \mu_0$, it is possible to discern by eye some patterns in the variation of the dipole moment with sphere radius. We can see that the in-phase and quadrature parts complement each other: the real parts show greater differences at higher frequencies, where the imaginary parts change less with size, and the imaginary parts vary more at lower frequencies, where the real parts change less. This general pattern is also noticeable for higher permeabilities, as the bottom panels of Fig. 1 show for $\mu = 100\mu_0$. Note that some cases where two different frequencies would yield a similar pattern in the imaginary part (at opposite sides of its maximum) actually show opposing variations in the real part. We expect the SVMs to be able to use this information.

In one experiment we use 200 training samples, with radii between 2.5 and 50 cm and permeabilities and conductivities random within a generous range, and then subject the SVMs to 2300 tests, inquiring whether $a \geq 25$ cm. We get success rates (defined as the ratio of correct answers to total number of tests) of about 97.7%, regardless of the algorithm used; the following is a typical breakdown:

SVM ^{light}	Predicted		mySVM	Predicted	
True ↓	+1	-1	True ↓	+1	-1
+1	991	38	+1	1008	21
-1	15	1256	-1	32	1239

(10)

We have also studied upright prolate spheroids under axial (parallel to $\hat{\mathbf{z}}$) or transverse (perpendicular to $\hat{\mathbf{z}}$) uniform excitation,³⁻⁵ respectively using β_z and β_t as discriminators. The patterns are less apparent in the presence of variable elongation, but some can still be found, mostly having to do with the quadrature (imaginary) response of the target.⁶ In general we expect axial excitation to give a better idea of the target size, while transverse excitation should be superior as a discriminator of elongation.

We have used the program **sphemi**⁵ to generate the dipole moments. When the solutions fail to converge (something that tends to happen at higher frequencies and is a consequence of finite machine precision), **sphemi** generates dipole moments in the SPA approximation, as described at the end of Sec. 2.

Excitation	Classification	SVM ^{light}	mySVM
Axial	$2a < 0.06$ m	87.00	90.62
Transverse	$2a < 0.06$ m	89.75	95.12
Axial and transverse	$2a < 0.06$ m	86.12	95.00
Axial	$e < 2.5$	62.25	69.50
Transverse	$e < 2.5$	62.38	58.00
Axial and transverse	$e < 2.5$	61.50	70.50

Table 1. SVM success rates (in percentage) for spheroids.

We have generated two data files: a 1000-sample training file and a 250-sample test file. In both of these, we let the diameter $2a$ vary at random between $2a = 0.015$ m and $2a = 0.15$ m and the elongation between $e = 1.001$ and $e = 5$; the relative permeability varies at random between $\mu_r = 50$ and $\mu_r = 150$, except that a third of the samples have $\mu_r = 1$. The conductivity is fixed at random at either $\sigma = 10^6$ S/m or $\sigma = 10^7$ S/m.

We first take the training file and ask the SVMs to discriminate by diameter and elongation for increasing values of these parameters, using axial data, transverse data, and both axial and transverse data. We use 200 training samples and 800 testing samples in each case. The results appear in Fig. 2. We can see that the classification by size is much more successful than that by elongation; it should be recalled when looking at the figure that a success rate of 50% corresponds to blind guessing. Also, the programs perform better at the ends of the range; this is not surprising, since in those cases most of the training samples have the same yes-or-no answer. Having both axial and transverse data tends to improve the performance, though not in all cases. Moreover, we can see, just as we expected, that transverse data is better than axial data for diameter discrimination. The opposite happens when studying elongation: axial data is more useful than transverse data. Table 1 gives some results in more detail.

Volume should be a robust discriminator, since it varies as the cube of the radius and only linearly with elongation. In our next experiment we want to see if it is possible to “overeducate” the SVM: *i.e.*, we want to know how the success rate is affected as the number of training samples increases beyond a certain point (we expect it to grow at the beginning, of course). We run both SVMs on our test file using sets of training samples ranging in size from 50 to 950 and ask them to determine if a given test sample has “volume” (defined here as $V = (2a)^3e$) larger than half the median, the median, twice the median, or four times the median within the testing file. In all cases we use both axial and transverse data. The results are in Fig. 3. We see that, as in Fig. 2, SVM^{light} gives the best results for very large volumes, while mySVM tends to perform as well or better in all other cases; the success rate stabilizes and does not degenerate with more training samples.

5. CONCLUSION

In this paper we have studied the degree to which one can train a Support Vector Machine to aid in the identification of unexploded ordnance by providing a fast classification scheme that will filter out promising UXO candidates that can then be explored using more-elaborate forward models. We have seen that the two open-source implementations yield reasonable estimates (especially regarding size) when fed synthetic data resulting from analytic solutions to the EMI equations.

In the experiments we have run we have seen that, even though SVM^{light} may fare better than mySVM for some classification tasks, mySVM is in general more effective and more efficient than SVM^{light}. Moreover, we have noticed that SVM^{light} takes a very long time to yield an answer in some instances, while mySVM never does. This seems to be a limitation inherent to SVM^{light}—since the program performs well when it is restarted and run with the same data sets—and it hampers its performance and reliability.

We note once again that the capacity C of the SVM and the width σ of the RBF kernel are adjustable parameters. In this paper we have kept them fixed at $C = 4000$ and $\sigma = 2$, the recommended values. In future work it should be possible to tweak these parameters to optimize the programs’ performance even further. Moreover, it is possible and necessary to incorporate other data, both synthetic^{6,7} and measured, that can be used by the program to enhance its decision-making capability.

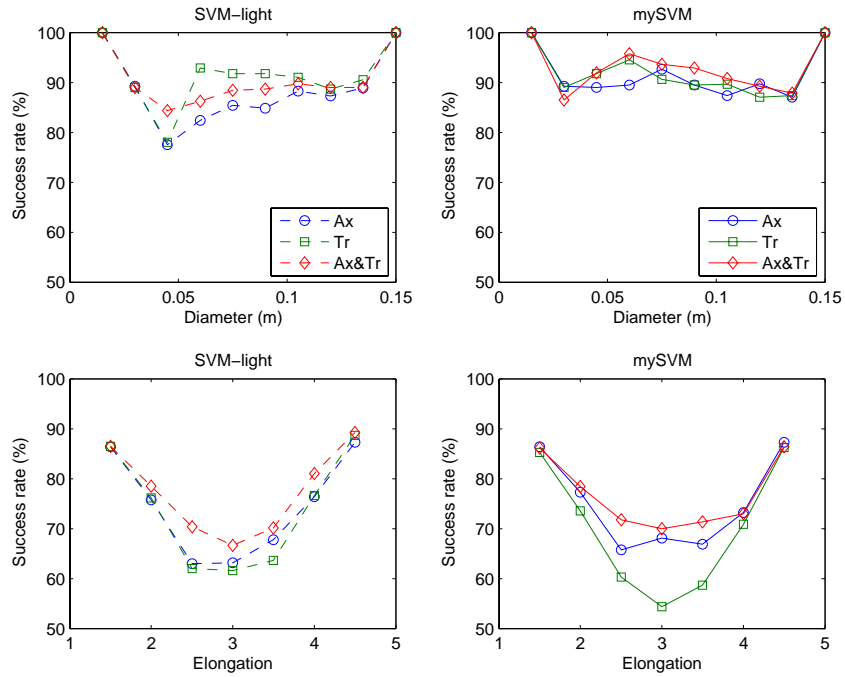


Figure 2. Success rates of SVM^{light} (dashed lines, left) and mySVM (full lines, right) in discriminating spheroids by diameter (top) and by elongation (bottom) for increasing values of these parameters using axial data only (circles), transverse data only (squares), and both axial and transverse data (diamonds). All experiments use 200 training samples and 800 tests.

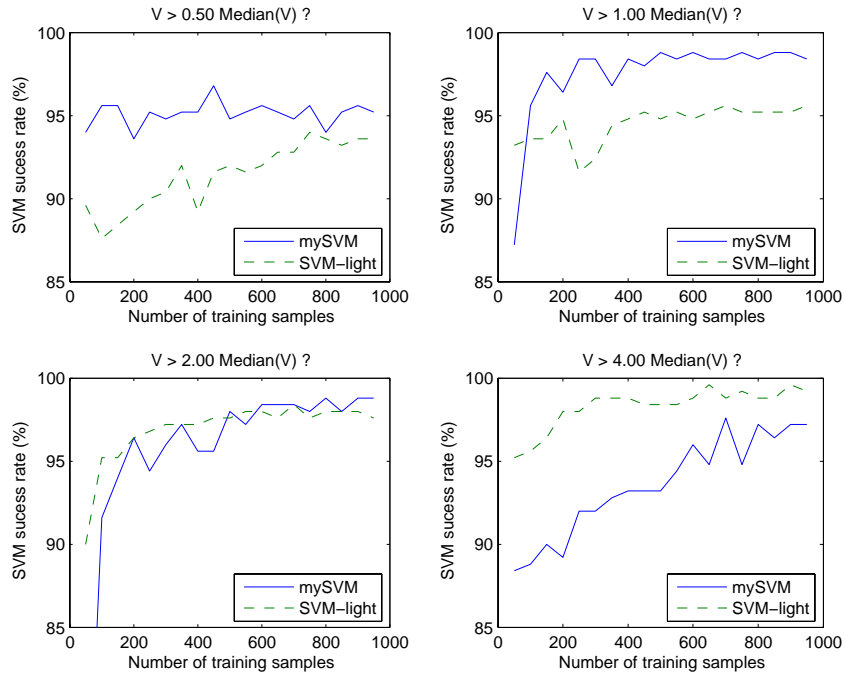


Figure 3. Success rates of mySVM (full lines) and SVM^{light} (dashed lines) in discriminating spheroids by volume—defined as $V \equiv (2a)^3 e$ —with increasing number of training samples. We classify the same 250 testing samples by inquiring whether they have volumes exceeding half the median, the median, twice the median, or four times the median.

Acknowledgment: This work was sponsored in part by the U.S. Army Corps of Engineers, Engineer Research and Development Center UXO EQ/I program, and by the Strategic Environmental Research and Development Program project #1443.

REFERENCES

1. C. E. Baum, ed., *Detection and Identification of Visually Obscured Targets*, Taylor & Francis, Philadelphia, 1999.
2. I. J. Won, D. A. Keiswetter, D. R. Hanson, E. Novikova, and T. M. Hall, "Gem-3: A monostatic broadband electromagnetic induction sensor," *J. Environ. Eng. Geophys.* **2**, pp. 53–64, Mar. 1997.
3. H. Braunisch, C. O. Ao, K. O'Neill, and J. A. Kong, "Magnetoquasistatic response of conducting and permeable prolate spheroid under axial excitation," *IEEE Trans. Geosci. Remote Sensing* **39**, pp. 2689–2701, Dec. 2001.
4. C. O. Ao, H. Braunisch, K. O'Neill, and J. A. Kong, "Quasi-magnetostatic solution for a conducting and permeable spheroid with arbitrary excitation," *IEEE Trans. Geosci. Remote Sensing* **40**, pp. 887–897, Apr. 2002.
5. B. E. Barrowes, K. O'Neill, T. M. Grzegorzczak, X. Chen, and J. A. Kong, "Broadband analytical magnetoquasistatic electromagnetic induction solution for a conducting and permeable spheroid," *IEEE Trans. Geosci. Remote Sensing* **42**, pp. 2479–2489, Nov. 2004.
6. F. Shubitidze, K. O'Neill, S. A. Haider, K. Sun, and K. D. Paulsen, "Application of the method of auxiliary sources to the wide-band electromagnetic induction problem," *IEEE Trans. Geosci. Remote Sensing* **40**, pp. 928–942, Apr. 2002.
7. F. Shubitidze, K. O'Neill, K. Sun, and K. D. Paulsen, "Investigation of broadband electromagnetic induction scattering by highly conductive, permeable, arbitrarily shaped 3-D objects," *IEEE Trans. Geosci. Remote Sensing* **42**, pp. 540–555, Mar. 2004.
8. L. Carin, H. Yu, Y. Dalichaouch, A. R. Perry, P. V. Czipott, and C. E. Baum, "On the wideband EMI response of a rotationally symmetric permeable and conducting target," *IEEE Trans. Geosci. Remote Sensing* **39**, pp. 1206–1213, June 2001.
9. N. Cristianini and J. Shawe-Taylor, *An Introduction to Support Vector Machines and other Kernel-Based Learning Methods*, Cambridge University Press, Cambridge, 2000.
10. T. Joachims, "Making large-scale SVM learning practical," in *Advances in Kernel Methods: Support Vector Learning*, B. Schölkopf, C. J. C. Burges, and A. J. Smola, eds., MIT Press, Cambridge, MA, 1998.
11. S. Rüping, "mySVM-Manual." <http://www-ai.cs.uni-dortmund.de/SOFTWARE/MYSVM/>, 2000.
12. A. Massa, A. Boni, and M. Donelli, "A classification approach based on SVM for electromagnetic subsurface sensing," *IEEE Trans. Geosci. Remote Sensing* **43**, pp. 2084–2093, Sept. 2005.
13. Y. Zhang, L. Collins, H. Yu, C. E. Baum, and L. Carin, "Sensing of unexploded ordnance with magnetometer and induction data: Theory and signal processing," *IEEE Trans. Geosci. Remote Sensing* **41**, pp. 1005–1015, May 2003.
14. M. N. Nabighian, ed., *Electromagnetic Methods in Applied Geophysics: Volume 1, Theory*, vol. 3 of *Investigations in Geophysics*, Society of Exploration Geophysicists, Tulsa, OK, 1997.
15. J. R. Wait, "A conducting sphere in a time varying magnetic field," *Geophysics* **16**, pp. 666–672, 1951.
16. S. J. Norton, W. A. SanFilipo, and I. J. Won, "Eddy-current and current-channeling response to spheroidal anomalies," *IEEE Trans. Geosci. Remote Sensing* **43**, pp. 2200–2209, Oct. 2005.
17. C. Flammer, *Spheroidal Wave Functions*, Stanford University Press, Stanford, CA, 1957.
18. C. Cortes and V. Vapnik, "Support-vector networks," *Machine Learning* **20**, pp. 273–297, Sept. 1995.
19. C. J. C. Burges, "A tutorial on Support Vector Machines for pattern recognition," *Data Mining and Knowledge Discovery* **2**, pp. 121–167, 1998.
20. J. C. Platt, "Probabilistic outputs for Support Vector Machines and comparisons to regularized likelihood ratios," in *Advances in Large Margin Classifiers*, A. J. Smola, P. Bartlett, B. Schölkopf, and D. Schuurmans, eds., MIT Press, Cambridge, MA, 1999.
21. K.-R. Müller, S. Mika, G. Rätsch, K. Tsuda, and B. Schölkopf, "An introduction to kernel-based learning algorithms," *IEEE Trans. Neural Netw.* **12**, pp. 181–202, Mar. 2001.